Viscoelastic response of Yukawa liquids

Z. Donkó,[1] J. Goree,[2] and P. Hartmann[1]
[1]*Research Institute for Solid State Physics and Optics, Hungarian Academy of Sciences, P.O. Box 49, H-1525 Budapest, Hungary*
[2]*Department of Physics and Astronomy, The University of Iowa, Iowa City, Iowa 52242, USA*
(Received 17 December 2009; published 14 May 2010)

The viscoelastic properties of strongly coupled Yukawa liquids are characterized by computing the complex shear viscosity $\eta(\omega)$. This is done using three methods of molecular-dynamics simulation: equilibrium, nonequilibrium, and Langevin dynamics, all with a mutually repulsive Yukawa interparticle potential. A change from viscous to elastic response is observed with increasing frequency, as well as a decrease of the magnitude of the viscosity with increasing frequency. The Langevin simulation reveals that the dependence of the complex viscosity on the friction has a different character for hot and cool liquids. At $\omega=0$, we find that as friction increases, the viscosity diminishes at high temperature but increases at low temperature. In addition to finding its frequency dependence, we also derive the wave-number (length-scale) dependence of the shear viscosity.

DOI: 10.1103/PhysRevE.81.056404 PACS number(s): 52.27.Gr, 52.25.Fi, 52.27.Lw, 83.60.Bc

I. INTRODUCTION

Viscoelasticity is the term used to describe how soft materials have both viscous and elastic properties. Viscosity describes an energy-loss mechanism, while elasticity involves energy storage. Most soft materials are viscoelastic since they exhibit both dissipative and elastic responses to disturbances.

A common way of characterizing viscoelasticity is decomposing the frequency-dependent viscosity into its real and imaginary components

$$\eta(\omega) = \eta'(\omega) - i\eta''(\omega). \tag{1}$$

The real part $\eta'(\omega)$ corresponds to viscous dissipation and the imaginary part $\eta''(\omega)$ corresponds to elasticity. The static viscosity $\eta(0)=\eta'(0)$ is intended for steady-flow patterns and its value is not accurate for flows with rapid time variations or short-scale lengths.

The system we consider consists of a collection of mutually repulsive charged particles that interact with a Yukawa (screened Coulomb) potential $\phi \propto (1/r)e^{-r/\lambda_D}$ (where λ_D is the screening length). Physical systems modeled this way include dusty plasmas and colloidal suspensions, which are both multiphase systems consisting of small particles of solid matter immersed in a partially ionized medium. The medium is either gas or liquid, whose molecules collide randomly with the solid particles, causing a frictional damping of the movement of the solid particles.

The collection of charged particles that we consider is termed a "strongly coupled plasma" when the interparticle potential energy exceeds the particle kinetic energy. This condition is quantified by the coupling parameter $\Gamma = Q^2/4\pi\epsilon_0 akT$, where Q is the charge of the particles, T is the temperature, and $a=(3/4\pi n)^{1/3}$ is the Wigner-Seitz radius for a number density n. When $\Gamma > 1$, we have a strongly coupled plasma, and collectively the particles behave like liquids or solids, with frequent collisions among neighboring particles. Two common types of strongly coupled plasmas are Yukawa systems ($\kappa=a/\lambda_D>0$, such as the one we model here) and the Coulomb one-component plasma ($\kappa=0$).

Transport properties of strongly coupled single- and multicomponent plasmas have attracted considerable interest during the past decades. The "static" (i.e., zero-frequency) shear viscosity η of these systems has been calculated by several authors and by means of a variety of theoretical and computational approaches [1–14]. A distinctive feature of the viscosity of both Coulomb and Yukawa liquids is a minimum at a certain temperature (or coupling, $\Gamma_{\min}$), unlike for most other liquids. This minimum arises from two mechanisms that contribute to the viscosity, described as the kinetic and potential terms, which vary oppositely with temperature [7].

Much of the current theoretical interest in viscosity of Yukawa systems has been stimulated by recent dusty plasma experiments, which have been performed with both two-dimensional monolayers and three-dimensional suspensions. Viscosity is different in two dimensions (2D) and three dimensions (3D), although in both cases there is a $\Gamma_{\min}$ for Yukawa systems. The viscosity and viscoelastic properties of 2D and quasi-2D suspensions have been investigated by several experimenters [15–25]. In [19], two counterpropagating laser beams were used to create a shear flow in a single dust layer in a plane Couette configuration, while in [24] a single laser beam was used to establish a shear flow in a multilayer dust system. In both experiments, the measured particle velocity profiles have been fitted to the solution of the Navier-Stokes equation, which provided kinematic viscosity values comparable to those obtained by MD simulations. Non-Newtonian behavior (shear thinning) of dust liquids has also been observed experimentally [15,16] and in MD simulations [14,26]. In [20], the shear elastic modulus of the plasma crystal and the viscosity contribution due to elasticity in the plasma liquid were estimated in an experiment carried out in magnetic field that caused a differential rotation of the particle cloud. Such combined viscous and elastic, i.e., viscoelastic, behavior of materials is an important topic of rheology and is often studied in material science.

The response to an oscillating shear characterizes the interaction at the molecular (or particle) level and the transport of momentum at different frequencies. At a microscopic scale, molecules remain attached to the same neighbors for a certain time, and during that time, they will rebound when disturbed and the microscopic motion will be elastic. At

longer time scales, due to thermal motions, a molecule can slip past its neighbors, irreversibly changing its location, and this contributes to viscosity. Thus, for most liquids, one expects elastic behavior to dominate at short-time scales and viscous behavior at long-time scales. The same is expected for spatial scales: elasticity in a liquid, which arises from molecules that rebound when disturbed in their position relative to their neighbors, will be limited to small distances on the order of the molecular spacing, whereas at long hydrodynamic distances, viscous behavior will dominate. Simulations are useful for studying these processes that occur at time and distance scales that are too small to be accessible for most experimental methods.

Here, our aim is to extend previous simulation efforts and to contribute to the understanding of the microscopic background of the viscoelastic response of Yukawa liquids. We calculate the frequency dependence, $\eta(\omega)$, and the length-scale dependence, $\eta(k)$, of the shear viscosity for 3D Yukawa liquids using three simulation methods:

(1) An equilibrium molecular-dynamics (EMD) simulation under steady and uniform conditions, where the microscopic fluctuations are used to compute viscosity.

(2) A nonequilibrium molecular-dynamics (NEMD) simulation with an applied oscillatory shear, where viscosity is determined from the resulting response, as measured in the time-dependent pressure tensor [27].

(3) A Langevin dynamics (LD) simulation, which includes friction and random forces to model the effect of collisions of background gas molecules with the charged particles of the Yukawa system.

Testing for agreement of the EMD and NEMD methods will serve the dual purposes of validating the codes and affirming the physical relationship between transport coefficients derived from microscopic observations both with and without macroscopic perturbations. Comparing the EMD and LD simulations will reveal the influence that randomizing collisions have on the complex viscosity. Details of these simulation techniques are presented in Secs. II and III, while results are presented in Sec. IV and summarized in Sec. V.

II. SIMULATION METHODS

In this section, we present the methods used in our simulations. This is, however, preceded by the definition of normalized units that will be used in the paper.

A. Units

For (inverse) temperature and screening length, we use the dimensionless parameters Γ and κ, which have already been introduced. Further normalized units are indicated by bars over the symbols:

(i) Length: $\bar{r}=r/a$.

(ii) Wave number: $\bar{k}=ka$.

(iii) Frequency: $\bar{\omega}=\omega/\omega_p$, where $\omega_p=(nQ^2/\epsilon_0 m)^{1/2}$ is the plasma frequency and m is the mass of a particle.

(iv) Correlation functions: $\bar{C}(t)=C(t)/C(0)$.

(v) Shear rate: $\bar{\gamma}=(dv_x/dy)(a/v_0)$, where $v_0=(2kT/m)^{1/2}$ is the thermal velocity.

(vi) Friction: $\bar{\nu}=\nu/\omega_p$.

(vii) Viscosity: $\bar{\eta}=\eta/mn\omega_p a^2$.

We note that some authors have used other normalizations, for example, the Einstein frequency instead of the plasma frequency when normalizing viscosity, e.g., [7]. The Einstein frequency corresponds to the harmonic motion of a particle trapped in a stationary cage consisting of its nearest neighbors.

B. Frequency dependence

Viscosity arises from shear stress, which is represented by the off-diagonal elements of the pressure tensor **P**. To investigate the frequency dependence of viscosity, $\eta(\omega)$, we will allow the pressure tensor to vary with time, $\mathbf{P}(t)$, either due to microscopic fluctuations under equilibrium conditions (in our EMD and LD simulations) or due to an applied oscillating shear (in our NEMD simulation). Making use of simulations that track the positions and velocities of all particles as a function of time, we compute the shear stress $P_{xy}(t)$ as

$$P_{xy}=\sum_{i=1}^{N}\left[mv_{ix}v_{iy}-\frac{1}{2}\sum_{j\neq i}^{N}\frac{x_{ij}y_{ij}}{r_{ij}}\frac{\partial\phi(r_{ij})}{\partial r_{ij}}\right], \tag{2}$$

where N is the number of particles, $r_{ij}=|\mathbf{r}_{ij}|=|\mathbf{r}_i-\mathbf{r}_j|=|(x_{ij},y_{ij})|$. From this shear stress, we will obtain the viscosity η. The different ways this is done in our simulation approaches are described next.

1. Equilibrium EMD simulation

In all our simulations, we integrate the equation of motion for particles to yield time histories of the positions and velocities of all particles. For our EMD simulation, the equation of motion of a particle i is

$$m\frac{d\mathbf{v}_i}{dt}=-Q\sum_{j\neq i}^{N}\nabla\phi_{ij}, \tag{3}$$

where ϕ_{ij} is the potential, for a binary Yukawa interaction, at the position of particle i due to particle j. In this equilibrium simulation, there are no externally applied forces. Boundary conditions are periodic and the simulation volume is a cube with edges of length L. Particles are initialized at random positions, and after the motion thermalizes, we record the time series of particle positions and velocities. No thermostat is used during the data-recording period.

After recording particle positions, we compute the shear stress, i.e., the off-diagonal element of the pressure tensor, using Eq. (2). We also compute the other off-diagonal elements $P_{xz}(t)$ and $P_{yz}(t)$.

Next, we calculate the autocorrelation function of the shear stress

$$C_\eta(t)=\langle P_{xy}(t)P_{xy}(0)\rangle. \tag{4}$$

Exploiting the symmetry of this simulation in the x, y, and z directions, we also compute $C_\eta(t)$ for the other off-diagonal elements and average them to improve the signal-to-noise ratio.

Finally, the complex viscosity $\eta(\omega)=\eta'(\omega)-i\eta''(\omega)$ is computed from $C_\eta(t)$ using the generalized Green-Kubo re-

lation. Unlike in the case of the usual Green-Kubo relation, which is used to compute the static viscosity by integrating $C_\eta(t)$ over time, here we seek the frequency-dependent viscosity. This is done using the Laplace-Fourier transform of $C_\eta(t)$ [28,29]

$$\eta(\omega) = \frac{1}{VkT}\int_0^\infty C_\eta(t)e^{i\omega t}dt, \tag{5}$$

where $V=L^3$ is the simulation volume. In practice, we replace the infinite integration limit with a finite time. Recognizing that $C_\eta(t)$ should remain positive in principle, but at large time it fluctuates about zero due to the finite system size, we choose the limit as the time when this noisy $C_\eta(t)$ first crosses zero.

2. Nonequilibrium NEMD simulation

For our NEMD method, we choose the homogeneous shear algorithm [30], which simulates a planar Couette flow. In this method, a shear is applied along one of the principal directions, perpendicularly to two opposite faces of the simulation cube. The other four faces of the cube do not have any applied shear. This method has frequently been used in studies of the viscosity parameters of liquids and is based on the Gaussian thermostated SLLOD equations of motion (6) in conjunction with the Lees-Edwards (sliding) periodic boundary conditions (for details, see [30]). The equations of motion are

$$\frac{d\mathbf{r}_i}{dt} = \frac{\tilde{\mathbf{p}}_i}{m} + \gamma y_i \hat{\mathbf{x}},$$

$$\frac{d\tilde{\mathbf{p}}_i}{dt} = \mathbf{F}_i - \gamma \tilde{p}_{yi}\hat{\mathbf{x}} - \alpha\tilde{\mathbf{p}}_i. \tag{6}$$

Here, $\tilde{\mathbf{p}}=(\tilde{p}_x,\tilde{p}_y)$ is the peculiar momentum of particles, $\hat{\mathbf{x}}$ is the unit vector in the x direction, and α is the Gaussian thermostat multiplier. The above set of equations is solved using an operator-splitting technique [31]. For static conditions ($\omega=0$), the method would yield the static viscosity, computed as $\eta=-\langle P_{xy}\rangle/\gamma$ in the limit of long recording time ($t\to\infty$) [30].

The method of computing η must be adapted for our case, where the applied shear $\gamma(t)$ is modulated [27] with time according to

$$\gamma(t) = \gamma_0 \cos(\omega t). \tag{7}$$

Since we use a harmonic modulation of $\gamma(t)$, the resulting shear stress (the off-diagonal element of the pressure tensor) also becomes a periodic function of the time. We calculate the complex η, Eq. (1), in three steps. First, we calculate the modulus $|\eta(\omega)|$ as the ratio of the harmonic amplitude of $P_{xy}(t)$ and the amplitude of the applied shear γ_0. The amplitude of $P_{xy}(t)$ is measured simply from its time series, for example, as in Fig. 1(a). Second, we compute the phase angle of $-P_{xy}(t)$ from a cross correlation of $-P_{xy}(t)$ with the applied shear, i.e., the two time series shown in Fig. 1(a). We note that this phase is the same as for η. Third, we combine the modulus and phase of η to yield the full complex value of η.

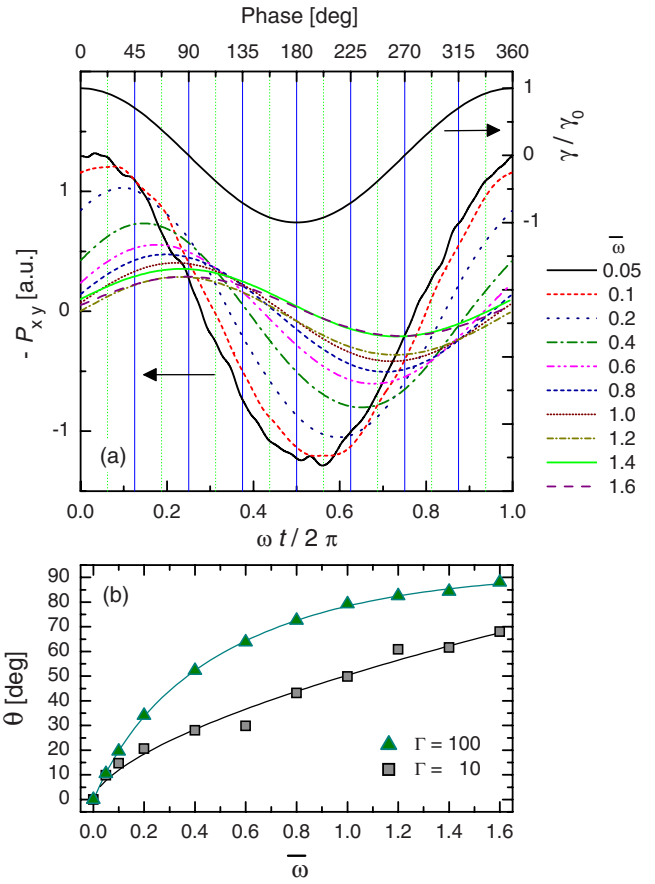

FIG. 1. (Color online) (a) Time-dependent shear rate $[\gamma(t)/\gamma_0 = \cos(\omega t)$, right scale] and off-diagonal element of the pressure tensor ($-P_{xy}$, left scale) at $\Gamma=100$ and $\kappa=1$ for a series of perturbation frequencies $\bar{\omega}$. (b) Phase delay θ between the excitation and the response of the system as a function of the frequency of the applied shear. We will compute η' and η'' for a given value of ω using both the modulus $|\eta|$ computed as the ratio of the amplitudes of the $-P_{xy}$ and γ wave forms shown in (a) and the phase found in (b).

In Fig. 1, we note that the response of the system, $-P_{xy}(t)$, lags behind the excitation $\gamma(t)$. The phase angle θ for this lag is plotted in Fig. 1(b). We see that it increases with the applied frequency, approaching a 90° lag at a high applied frequency ω. This phase lag indicates a transition from viscous to elastic response as frequency is increased. We also see in Fig. 1(a) that the amplitude of $P_{xy}(t)$ decreases with increasing frequency; this indicates that $|\eta|$ decreases with frequency. These are two of the main properties of the viscoelastic system: as the applied frequency increases, there is a transition from viscous to elastic response and the magnitude of the η diminishes. (We will soon confirm the transition to elastic behavior in a more intuitive way using plots of $\eta'(\omega)$ and $\eta''(\omega)$ obtained from the EMD simulation).

Note that in these results for the NEMD, ω is always an applied frequency. This is unlike the case of the EMD simulation where ω is the variable in the Laplace-Fourier transform, Eq. (5).

3. Langevin simulation

The Langevin simulation is similar to the EMD simulation, except that frictional damping and random forces are

included in the equation of motion. The friction and random forces model the effect of random collisions of gas molecules with the charged particles. The equation of motion for a particle i is

$$m\frac{d\mathbf{v}_i}{dt} = -Q\sum_{j\neq i}^{N}\nabla\phi_{ij} - \nu m\mathbf{v} + \mathbf{R}, \tag{8}$$

where ϕ_{ij} is the Yukawa interaction potential, ν is the frictional damping, and $\mathbf{R}$ is a random force. The damping term $-\nu m\mathbf{v}$ accounts for the average effect of collisions with gas molecules, while the stochastic force $\mathbf{R}$ emulates the individual random kicks in these collisions. In solving the above equation, we follow the Beeman-like method of [32,33]. During the course of the simulation, we measure the off-diagonal elements of the pressure tensor and apply the generalized Green-Kubo relation to derive the complex viscosity, as in our EMD simulations.

C. Wave-number dependence

To find the wave-number dependence of viscosity, $\eta(k)$, we use the particle time series to calculate the transverse microscopic current, τ_{xy},

$$\tau_{xy}(k,t) = \sum_{j=1}^{N} v_{xj}e^{iky_j}. \tag{9}$$

We also compute τ_{yx}, τ_{xz}, τ_{zx}, τ_{zy}, and τ_{yz} and we will exploit the symmetry of the EMD simulation by averaging these six functions to improve the signal-to-noise ratio. Data for τ are collected in the same EMD simulation runs as for the elements of $\mathbf{P}$.

Following the method of [34,35], we next compute the autocorrelation function of the transverse current

$$C_T(\bar{k},t) = \langle \tau_{xy}(\bar{k},t)\tau_{xy}^*(\bar{k},0)\rangle, \tag{10}$$

and finally, according to Eq. (7) of [35], the wave-number-dependent viscosity as

$$\eta(\bar{k}) = \frac{nm}{k^2}\left[\int_0^\infty \bar{C}_T(\bar{k},t)dt\right]^{-1}, \tag{11}$$

where $\bar{C}_T(\bar{k},t)=C_T(\bar{k},t)/C_T(\bar{k},0)$. The infinite integration limit in Eq. (11) is replaced in our calculation with $\omega_p t = 800$.

Because of the finite width L of our simulation cube, we will evaluate all functions of wave number at discrete values. Allowed values of k are integer multiples of $2\pi/L$, and for the normalized wave number $\bar{k}$, allowed values are multiples of $\bar{k}_{\min}=2\pi a/L$. Our results for $\tau(\bar{k},t)$, $C_T(\bar{k},t)$, and $\eta(\bar{k})$ are evaluated at these discrete values.

III. SIMULATION PARAMETERS

The physical parameters that are the inputs to the simulation are primarily Γ and κ. For most of the results reported in Sec. IV, we will use only $\kappa=1$, which is a value typical for dusty plasma experiments. For the NEMD simulations, the physical parameters also include the frequency ω (or $\bar{\omega}=\omega/\omega_p$ in dimensionless units) and the amplitude of the applied shear $\bar{\gamma}$.

Numerical parameters in the simulations include the particle number N, the time step and length of the simulation runs, and a cutoff radius for computing the interparticle forces. As is often the case with three-dimensional simulations, the computational cost requires that we use a rather small simulation volume. Most of our EMD simulations are carried out using $N=2197$ particles, which corresponds to a length $L\cong 21a$ for the computational box. To check for system-size effects, we repeated some of our EMD and NEMD runs with an 8 times larger system size, $N=17\,576$. The time step was $\Delta t \leq 0.03/\omega_p$. At the beginning of the simulation, we waited for the system to thermalize before recording data; this waiting period was 10^5 time steps in the case of $N=2197$ particles. We then recorded data for 10^6 time steps. In the case of 17 576 particles, data were recorded for 5×10^5 time steps.

In the NEMD simulations, we apply a desired perturbation frequency. We repeated the simulation for various values in the range $0\leq\bar{\omega}\leq 1.6$. Before recording data, we waited for the system to reach a steady oscillation; this waiting time was 200 cycles, i.e., $\omega t=400\pi$. We then recorded data for the next 400 perturbation cycles. Results from the NEMD simulation (shear stress and viscosity) represent averages over these 400 cycles. An 8 times larger system was also simulated with this method for a few parameter combinations; for these runs, the number of measurement cycles ranged between 300 and 400.

For the Langevin simulation, we specify the friction ν and the corresponding magnitude of the random force in Eq. (8). We chose frictional damping values in the range $0.001\leq\bar{\nu}\leq 0.3$, which includes values of interest for dusty plasma experiments [36,37]. We used 2197 particles. The length of data recording was 10^6 time steps, following a waiting period of 10^5 time steps.

As a validity check for our EMD and Langevin simulations, we verified that the conditions of our simulations reasonably modeled thermal equilibrium. We calculated the variance in the time series for temperature and compared this to the canonical fluctuation level for a finite-size thermodynamic system [38]. We found that our variance was satisfactory, exceeding the canonical level by less than 1%.

IV. RESULTS AND DISCUSSION

A. Frequency dependence

One of our chief results is the frequency dependence of the complex viscosity $\eta(\omega)$, which we evaluate in terms of the real part (viscosity) $\eta'(\omega)$ and imaginary part (elasticity) $\eta''(\omega)$. Results from both our EMD and NEMD simulations are presented in Fig. 2. All results are for $\kappa=1$. Results from the NEMD simulation are shown as data points because they were performed at specific frequencies for the applied shear, while the data for the EMD simulations are shown as smooth curves as functions of ω. (For the NEMD simulations, ω is a specified excitation frequency, while for the other two simu-

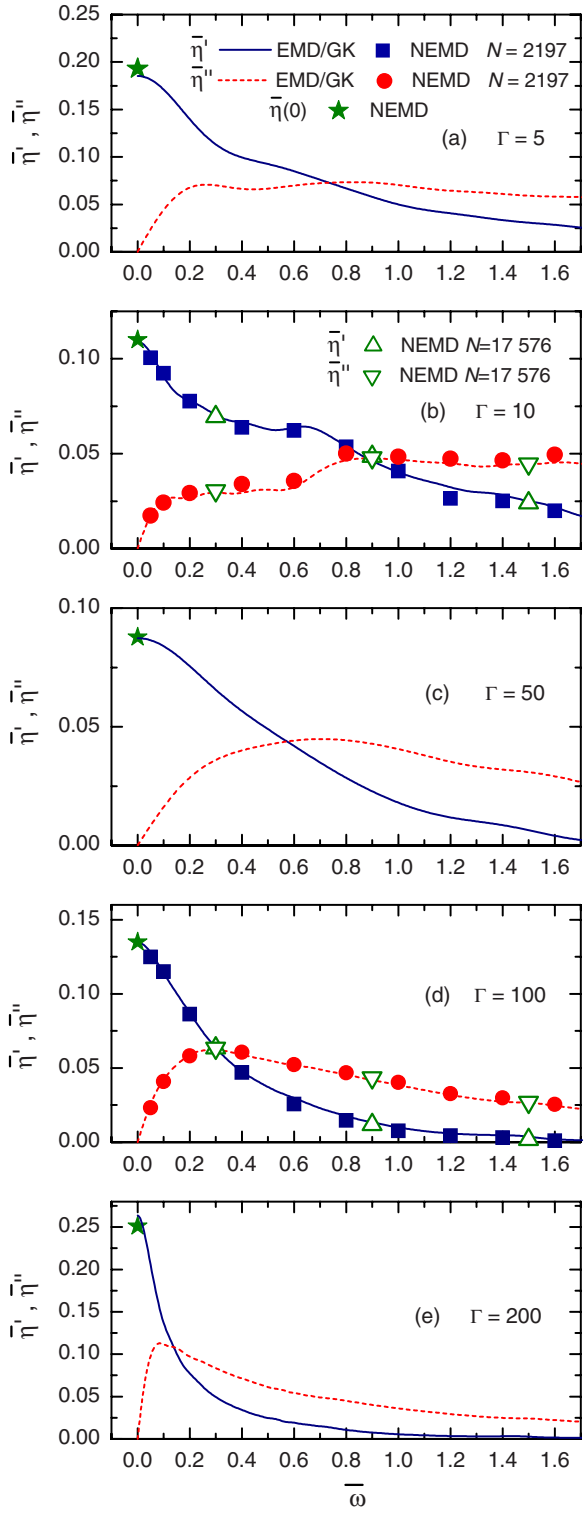

FIG. 2. (Color online) Complex viscosity $\bar{\eta}(\omega)=\bar{\eta}'(\omega)-i\bar{\eta}''(\omega)$ from our EMD and NEMD simulations. Results are shown for different values of the coupling parameter, always at $\kappa=1$. EMD results in conjunction with the generalized Green-Kubo relation: solid blue line: real part; dashed red line: imaginary part. NEMD results with $N=2197$ particles: filled blue squares: real part; filled red circles: imaginary part. NEMD results with $N=17\,576$ particles: open up triangles: real part; open down triangles: imaginary part. For comparison, the stars indicate static $\bar{\eta}(0)$ NEMD results from Ref. [14].

lation methods, it is a continuous variable resulting from the Fourier transform of the time series data.)

One reason that it is useful to perform both EMD and NEMD simulations is that their results can be compared as a validation test. Examining Fig. 2, we find good agreement between these methods: the data points for NEMD coincide with the smooth curves for EMD. The EMD data shown in Fig. 2 are averages of eight simulation runs, while the NEMD data originate from single simulation runs at the given frequencies.

Another reason to compare NEMD and EMD simulations is to affirm the physical relationship between transport coefficients derived with and without the presence of macroscopic gradients. While the equations of motion in the two methods are very similar, the viscosity is computed from the pressure tensor at quite different conditions, with (NEMD) and without (EMD) macroscopic shear. The agreement seen in Fig. 2 affirms that viscosity derived both ways have the same values, for all frequencies studied here.

We find that the dissipative (real) part of the viscosity $\bar{\eta}'$ decreases with frequency. This is observed in Fig. 2 for all Γ values that we tested.

The elastic (imaginary) part $\bar{\eta}''$ at first increases with frequency well below the plasma frequency ω_p. It then has a maximum and diminishes with frequency. The maximum of $\bar{\eta}''$ is most definitive for high Γ, while for lower values of Γ, we find that $\bar{\eta}''$ flattens within the frequency range studied. In general, the maximum occurs at a frequency that decreases with Γ.

For the frequency dependence of the viscosity, we have carried out different validation tests:

(1) We note agreement of our results with previously reported simulations for static viscosity. In the limit of $\bar{\omega}\to 0$, our results for the real part η' agree with NEMD results [14] for static viscosity, indicated with a star in the panels of Fig. 2.

(2) For selected frequencies ($\bar{\omega}=0.3$, 0.9, and 1.5), we have also run the NEMD code with $N=17\,576$ particles; agreement between these data in Fig. 2 shows no significant system-size effects.

(3) Comparison of the results of our EMD simulations carried out with $N=2197$ and 17 576 particles for selected (Γ,κ) pairs, displayed in Fig. 3, shows no significant system-size effects.

To reveal the richness of the dependence of η on both Γ and ω, we present Fig. 4. The viscous part η' and elastic parts η'' are shown as color maps in the top and bottom panels, respectively, for many more values of Γ than in Fig. 2. For the viscous part η', we find that the minimum viscosity at low frequency vanishes at higher frequencies. To see this, we direct the reader's attention to vertical profiles in panel (a): at low frequency $\bar{\omega}\ll 1$, the viscosity has a minimum with respect to Γ, at $\Gamma\approx 30$ as was previously known, but for higher frequencies $\bar{\omega}>0.3$, this minimum vanishes and the viscous part η' decays monotonically with Γ.

We can identify an underlying physical reason for the disappearance of the minimum viscosity η' in Fig. 4. Recall that the Green-Kubo approach offers the insight that the viscosity has two major contributions, kinetic and potential. In the static case $\omega=0$, it is well known that these terms vary

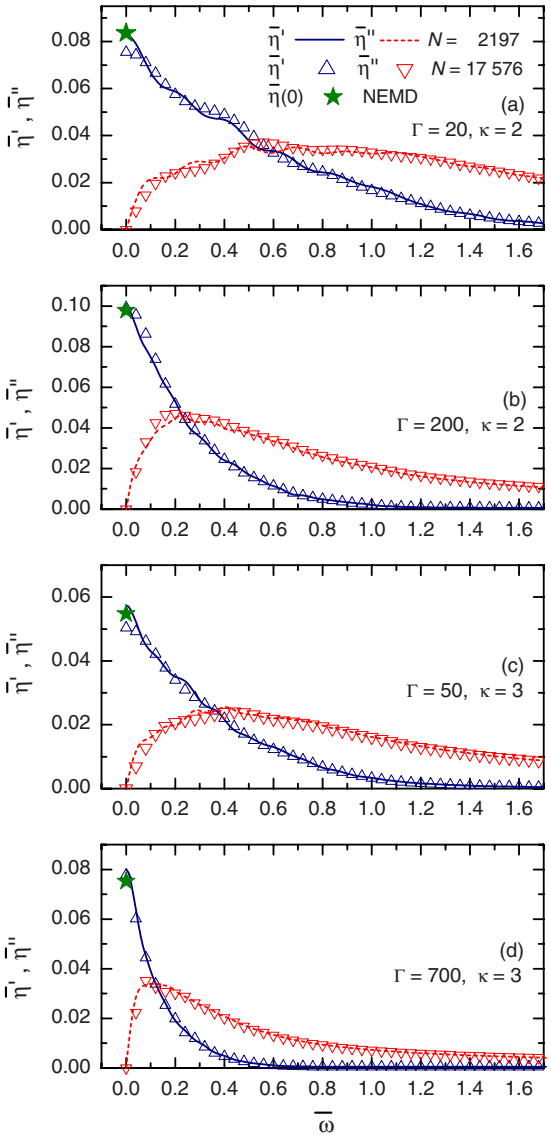

FIG. 3. (Color online) Complex viscosity $\bar{\eta}(\omega)=\bar{\eta}'(\omega)-i\bar{\eta}''(\omega)$ from our EMD simulations for different values of the coupling and screening parameters. $N=2197$ particles: solid blue line: real part; dashed red line: imaginary part. $N=17\,576$ particles: open up triangles: real part; open down triangles: imaginary part. Stars indicate static $\bar{\eta}(0)$ NEMD results from Ref. [14].

oppositely with Γ: the kinetic term is large for high temperatures (low Γ) and diminishes as the temperature is reduced, while the potential term has the opposite dependences. For the static case, a minimum viscosity occurs approximately where these two contributions are equal. Our result here is that this minimum vanishes at higher frequency and the viscosity η' varies inversely with Γ. This inverse dependence indicates that at high ω, the kinetic term is dominant for all values of Γ. In other words, we find that the potential term becomes insignificant as $\bar{\omega}$ increases above unity, i.e., as ω increases above ω_p. For the elastic part, $\bar{\eta}''$, we find in Fig. 4(b) that it too has minimum with respect to Γ at low frequencies. As it was for the viscous part $\bar{\eta}'$, this minimum vanishes at higher frequencies. The clarification of this complex behavior of $\bar{\eta}'$ and $\bar{\eta}''$ could be well aided by an analytical model, which is beyond the scope of this paper.

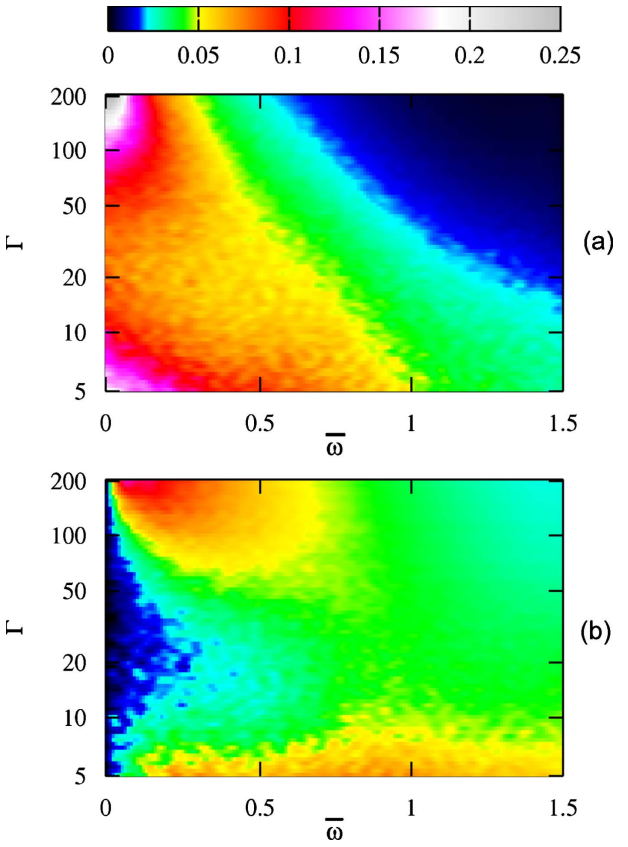

FIG. 4. (Color online) Complex viscosity $\bar{\eta}(\Gamma,\omega)$ from our EMD simulations for $5\leq\Gamma\leq200$ and $\kappa=1$. (a) Viscous part $\bar{\eta}'$. (b) Elastic part $\bar{\eta}''$.

We next explore the effects of friction and random forces as revealed by our LD (Langevin dynamics) simulation. Figures 5(a) and 5(b) compare the results for $\bar{\eta}(\omega)$ from the LD and the frictionless EMD simulation, for $\kappa=1$. Here, the friction level was chosen to have a relatively high value $\bar{\nu}=0.3$. For the higher-temperature case of $\Gamma=10$ in panel (a), the effect is mostly to reduce the elastic part $\bar{\eta}''$ for all frequencies and the viscous part $\bar{\eta}'$ at low frequencies. For the lower-temperature case of $\Gamma=100$ in panel (b), the effects of friction and random forces have a greater frequency dependence: the viscous and elastic parts are both suppressed at high frequencies and enhanced at low frequencies, as compared to the frictionless case.

Since the most profound effects of friction are shown in Figs. 5(a) and 5(b) to occur at low frequencies, we examine the $\omega=0$ case more closely in panel (c). The effect of damping is small for values $\bar{\nu}\lesssim10^{-2}$ where $\bar{\eta}(0)$ is almost constant, but it becomes progressively more profound at higher-damping values. This profound dependence on damping rate has opposite tendencies for high and low Γ.

The physical reason for this contrasting behavior is the opposite response of the kinetic and potential contributions to the viscosity on the increased friction. We found that in our simulations, the kinetic term decreases with increasing friction, while the potential term does the opposite and increases with increasing friction. This result is in agreement

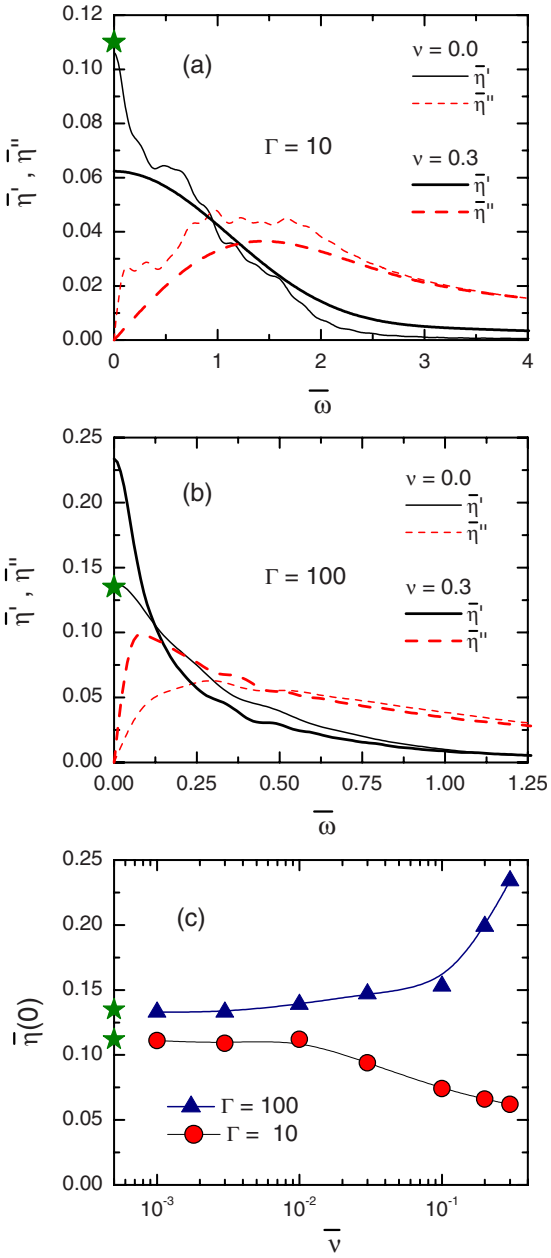

FIG. 5. (Color online) LD and EMD results compared for the complex viscosity $\bar{\eta}(\omega)=\bar{\eta}'(\omega)-i\bar{\eta}''(\omega)$. In (a) and (b), results for finite friction $\bar{\nu}=0.3$ are from LD and are shown with thick lines, while $\bar{\nu}=0$ results from EMD are shown with thin lines (solid lines: real part; dashed lines: imaginary part). Results are presented for $\Gamma=10$ in (a) and for a lower-temperature case $\Gamma=100$ in (b). In (c), the friction dependence at zero frequency of the viscous part $\bar{\eta}'(0)$ is shown to depend differently on damping, depending on whether the value of Γ is high or low. The latter effect is attributed to the opposite roles of the kinetic and potential terms. Stars are data points for the $\bar{\nu}=0$ NEMD results from Ref. [14].

with the earlier findings of [13]. While the origin of this behavior is discussed in the papers of Ramazanov and Dzhumagulova [13] and in Vorona *et al.* [39], we feel that additional simulation and theoretical efforts are required to uncover the underlying physical effects.

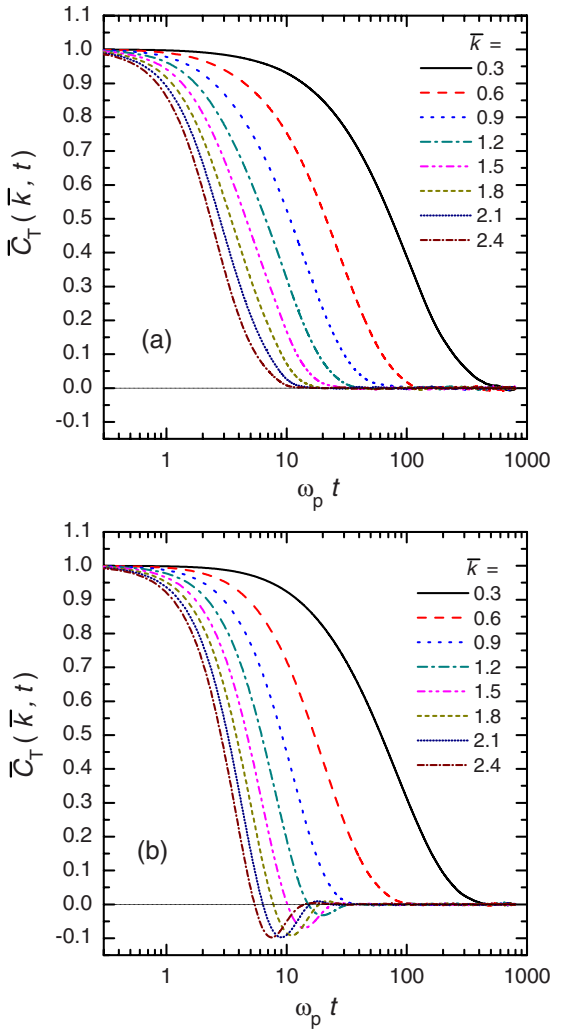

FIG. 6. (Color online) Normalized transverse current autocorrelation functions $\bar{C}_T(\bar{k},t)$ for (a) $\Gamma=10$ and (b) $\Gamma=100$ for a series of wave numbers. Note the appearance of a negative peak at higher wave numbers in (b).

B. Wave-number dependence

We now turn to the dependence of viscosity on wave number. We will first present our results for the autocorrelation functions of the transverse current and identify their physically significant features. We will then use these autocorrelation functions to compute the viscosity and its dependence on wave number.

Autocorrelation functions of the transverse current from our EMD simulation are presented in Fig. 6. As mentioned in Sec. II C, allowed wave numbers in our simulation cube of finite size L are at discrete values. They are integer multiples of $\bar{k}_{\min}=2\pi a/L\cong 0.3$.

We find that our autocorrelation function decays, but not exactly exponentially with time. Previous simulations for non-Yukawa liquids [34] showed monotonic decreases of C_T at small time and high temperatures that is often compared to the theoretical predictions for a hydrodynamic approximation. In this hydrodynamic approximation, an exponential decay $\bar{C}_T=\exp(-\bar{\eta}\bar{k}^2\omega_p t)$ is anticipated. This prediction, when

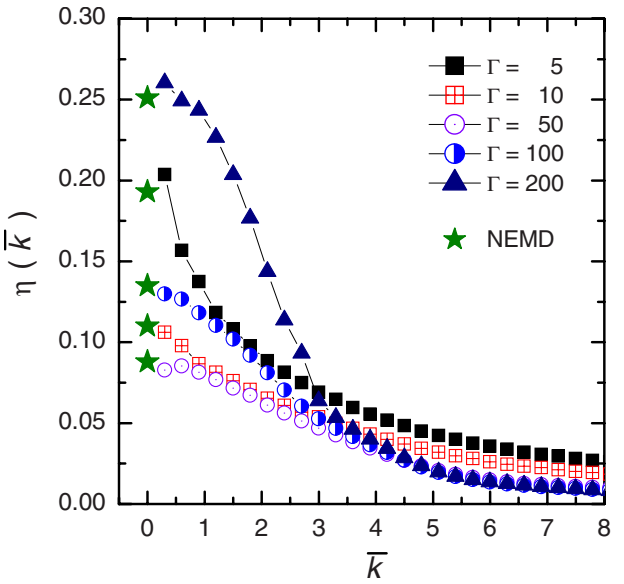

FIG. 7. (Color online) Wave-number dependence of the static viscosity obtained from the EMD simulation for different values of the coupling parameter and $\kappa=1$. NEMD refers to viscosity values obtained with the homogeneous shear algorithm [14].

it is obeyed, is sometimes used to fit the correlation function and thereby compute the viscosity η. We do not attempt to find η in this manner because the monotonic decay at small time in our results in Fig. 6 is exponential only at low wave numbers. However, for a combination of higher wave numbers and low temperatures, the autocorrelation functions generally show a nonmonotonic feature: a negative peak. We verified that the negative peak is not a spurious result by performing a system-size check (with an 8 times increased number of particles, $N=17\,576$ at $\kappa=2$ and 3). Previous authors have interpreted this negative peak as the signature of transverse (shear) waves [34].

We now compute the shear viscosity η from the autocorrelation of the transverse current, $C_T(\bar{k},t)$, using Eq. (11). The results in Fig. 7 reveal a monotonic decay of $\eta(\bar{k})$. At high wave numbers, this decay nearly obeys a power law: $\bar{\eta}\propto 1/\bar{k}$ for small Γ and a more rapid $\bar{\eta}\propto 1/\bar{k}^2$ for large Γ.

As a validation, we compare our results at small $\bar{k}$, i.e., long wavelength, to the previously reported literature for the static viscosity. These previously reported static values, which were determined [14] using an NEMD simulation at zero frequency, are shown with a star symbols in Fig. 7. We find good agreement with our previous NEMD results for $\bar{\eta}(\bar{k})$ at small $\bar{k}$, lending confidence to our $\bar{\eta}(\bar{k})$.

V. SUMMARY

We have investigated the complex viscosity $\eta(\omega)$ and the wave-number-dependent viscosity $\eta(k)$ of 3D Yukawa liquids, which are measures of the viscoelasticity of the medium. They were computed using (i) an EMD simulation under steady and uniform conditions, (ii) a NEMD simulation with an applied oscillatory shear, and (iii) a LD simulation, which includes the effect of the background environment of gas and plasma on the Yukawa system. The equilibrium simulation made it possible to derive $\eta(\omega)$ via the generalized Green-Kubo relation, while the nonequilibrium approach that applies a harmonic perturbation to the system provided the modulus and the phase of the complex viscosity. We have observed the change from viscous to elastic response with increasing frequency, as well as a decrease of the magnitude of the viscosity with increasing frequency. Both the elastic and viscous parts of the viscosity have a minimum with respect to Γ at low frequency, but these minima vanish at higher frequency. The Langevin simulation revealed the dependence of the complex viscosity on the friction: we have found that with increasing friction the static viscosity $\bar{\eta}(0)$ decreases at low Γ and increases at high Γ. Analysis of the transverse current correlation functions showed the onset of nonhydrodynamic behavior at high Γ and intermediate wave numbers. As an integral of $\bar{C}_T(\bar{k},t)$, we have determined the wave-number (length-scale) -dependent viscosity $\bar{\eta}(\bar{k})$. In a future paper, we intend to develop indicators of the range of wave numbers that can be sustained for shear waves in a liquid using the negative peak in C_T.

ACKNOWLEDGMENTS

We thank Bin Liu and Lu Jing Hou for useful discussions. This work has been supported by the Hungarian Fund for Scientific Research through the Grants No. OTKA-K77653, No. PD75113, and No. MTA-NSF/102. This paper was supported by the Janos Bolyai Research Scholarship of the Hungarian Academy of Sciences. Work in the U.S. was supported by the National Science Foundation and NASA.

[1] P. Vieillefosse and J. P. Hansen, Phys. Rev. A **12**, 1106 (1975).
[2] J. Wallenborn and M. Baus, Phys. Lett. A **61**, 35 (1977); Phys. Rev. A **18**, 1737 (1978).
[3] B. Bernu, P. Vieillefosse, and J. P. Hansen, Phys. Lett. A **63**, 301 (1977); B. Bernu and P. Vieillefosse, Phys. Rev. A **18**, 2345 (1978).
[4] Z. Donkó and B. Nyíri, Phys. Plasmas **7**, 45 (2000).
[5] S. Bastea, Phys. Rev. E **71**, 056405 (2005).
[6] J. G. Clérouin, M. H. Cherfi, and G. Zérah, Europhys. Lett. **42**, 37 (1998).
[7] T. Saigo and S. Hamaguchi, Phys. Plasmas **9**, 1210 (2002).
[8] M. S. Murillo, Phys. Rev. E **62**, 4115 (2000).
[9] G. Faussurier and M. S. Murillo, Phys. Rev. E **67**, 046404 (2003).
[10] K. Y. Sanbonmatsu and M. S. Murillo, Phys. Rev. Lett. **86**, 1215 (2001).

[11] G. Salin and J.-M. Caillol, Phys. Rev. Lett. **88**, 065002 (2002); Phys. Plasmas **10**, 1220 (2003).
[12] O. S. Vaulina and I. E. Dranzhevski, Phys. Scr. **73**, 577 (2006); Plasma Phys. Rep. **33**, 494 (2007).
[13] T. S. Ramazanov and K. N. Dzhumagulova, Contrib. Plasma Phys. **48**, 357 (2008).
[14] Z. Donkó and P. Hartmann, Phys. Rev. E **78**, 026408 (2008).
[15] C. L. Chan, W. Y. Woon, and Lin I, Phys. Rev. Lett. **93**, 220602 (2004).
[16] A. V. Ivlev, V. Steinberg, R. Kompaneets, H. Höfner, I. Sidorenko, and G. E. Morfill, Phys. Rev. Lett. **98**, 145003 (2007).
[17] M. Kretschmer, H. Höfner, M. Thoma, M. Fink, S. Ratynskaia, G. Morfill, K. Tarantik, V. Fortov, O. Petrov, A. Usachev, A. Zobnin, and Yu. Gerasimov, AIP Conf. Proc. **799**, 235 (2005).
[18] G. Morfill, S. Khrapak, A. Ivlev, and B. Klumov, Phys. Scr., **T107**, 59 (2004).
[19] V. Nosenko and J. Goree, Phys. Rev. Lett. **93**, 155004 (2004).
[20] U. Konopka, D. Samsonov, A. V. Ivlev, J. Goree, V. Steinberg, and G. E. Morfill, Phys. Rev. E **61**, 1890 (2000).
[21] Ch.-L. Chan, Ch.-W. Io, and Lin I, Contrib. Plasma Phys. **49**, 215 (2009).
[22] W. T. Juan, M. H. Chen, and Lin I, Phys. Rev. E **64**, 016402 (2001).
[23] Ch.-L. Chan and Lin I, Phys. Rev. Lett. **98**, 105002 (2007).
[24] O. S. Vaulina, O. F. Petrov, A. V. Gavrikov, X. G. Adamovich, and V. E. Fortov, Phys. Lett. A **372**, 1096 (2008).
[25] C.-W. Io and Lin I, Phys. Rev. E **80**, 036401 (2009).
[26] Z. Donkó, J. Goree, P. Hartmann, and K. Kutasi, Phys. Rev. Lett. **96**, 145003 (2006).
[27] H. Komatsugawa and S. Nosé, Phys. Rev. E **51**, 5944 (1995).
[28] J.-P. Hansen and I. R. McDonald, *Theory of Simple Liquids* (Academic Press, New York, 1976).
[29] R. Zangi and L. J. Kaufman, Phys. Rev. E **75**, 051501 (2007).
[30] D. J. Evans and G. P. Morriss, *Statistical Mechanics of Non-equilibrium Liquids* (Academic Press, New York, 1990).
[31] G. Pan, J. F. Ely, C. McCabe, and D. J. Isbister, J. Chem. Phys. **122**, 094114 (2005).
[32] L. J. Hou and Z. L. Mišković, e-print arXiv:0806.3912.
[33] L. J. Hou, Z. L. Mišković, A. Piel, and P. K. Shukla, Phys. Plasmas **16**, 053705 (2009).
[34] U. Balucani, J. P. Brodholt, P. Jedlovszky, and R. Vallauri, Phys. Rev. E **62**, 2971 (2000).
[35] U. Balucani, R. Vallauri, and T. Gaskell, Phys. Rev. A **35**, 4263 (1987).
[36] Bin Liu, J. Goree, and Yan Feng, Phys. Rev. E **78**, 046403 (2008); B. Liu, J. Goree, V. Nosenko, and L. Boufendi, Phys. Plasmas **10**, 9 (2003).
[37] G. J. Kalman, M. Rosenberg, and H. E. DeWitt, Phys. Rev. Lett. **84**, 6030 (2000).
[38] B. L. Holian, A. F. Voter, and R. Ravelo, Phys. Rev. E **52**, 2338 (1995).
[39] N. A. Vorona, A. V. Gavrikov, A. S. Ivanov, O. F. Petrov, V. E. Fortov, and I. A. Shakhova, J. Exp. Theor. Phys. **105**, 824 (2007).